Dynamics of spatially nonuniform patterning in the model of blood coagulation

V. I. Zarnitsina and F. I. Ataullakhanov[a)]
National Research Center for Hematology, Russian Academy of Medical Sciences, Novozykovskii proezd 4a, Moscow, 125167 Russia

A. I. Lobanov
Department of Applied Mathematics, Moscow Institute of Physics and Technology, Institutskii pereulok 9, Dolgoprudny, 141700 Russia

O. L. Morozova
Institute of Control Sciences, Russian Academy of Sciences, Profsoyuznaya 65, Moscow, 117342 Russia

(Received 19 July 2000; accepted for publication 11 December 2000)

We propose a reaction-diffusion model that describes in detail the cascade of molecular events during blood coagulation. In a reduced form, this model contains three equations in three variables, two of which are self-accelerated. One of these variables, an activator, behaves in a threshold manner. An inhibitor is also produced autocatalytically, but there is no inhibitor threshold, because it is generated only in the presence of the activator. All model variables are set to have equal diffusion coefficients. The model has a stable stationary trivial state, which is spatially uniform and an excitation threshold. A pulse of excitation runs from the point where the excitation threshold has been exceeded. The regime of its propagation depends on the model parameters. In a one-dimensional problem, the pulse either stops running at a certain distance from the excitation point, or it reaches the boundaries as an autowave. However, there is a parameter range where the pulse does not disappear after stopping and exists stationarily. The resulting steady-state profiles of the model variables are symmetrical relative to the center of the structure formed. © *2001 American Institute of Physics.* [DOI: 10.1063/1.1345728]

The stationary spatially nonuniform solution was first described by Turing,[1] and subsequently by others for several reaction-diffusion systems.[2–7] In almost all cases, the stationary nonuniform state reflects a balance between nonlinear self-accelerated and dissipative processes. All these dissipative stationary patterns are observed only if the diffusion coefficients of the variables differ significantly (i.e., the activator and its inhibitor are slow and fast, respectively).[3,8,9] Can stationary, spatially nonuniform patterns form in the reaction-diffusion systems in which the diffusion coefficients for all components are the same? Here we describe such mechanism of pattern formation, which we uncovered when studying the molecular events of blood coagulation. Our analysis of the blood coagulation pathways revealed that blood should be viewed as a reaction-diffusion system with complex kinetics due to the presence of several negative and positive feedbacks. This biochemical complexity leads to various unusual self-organization phenomena. To better understand the spatial dynamics of blood clotting, we have developed several mathematical models. One of the models containing the detailed description of the molecular events of clotting has a stationary, spatially nonuniform solution. The reduced model, which includes three chemical components with equal diffusion coefficients, also describes such a type of pattern formation. Here, we present the results of analysis of the reduced model.

I. INTRODUCTION

We have previously proposed that blood should be viewed as a biactive medium.[10,11] This hypothesis led to a phenomenological model describing formation of various spatially nonuniform structures.[12,13] The mechanism of their formation differed from Turing's mechanism, because an activator and its inhibitor had equal diffusion coefficients in this model. In both one- and two-dimensional cases, localized or regular periodic structures were formed by the indicative variable (which was defined as an integral of the activator over time).[12,13] In the two-dimensional case, the initial perturbation area (i.e., the area of an increased activator concentration) decayed into several localized lens-shaped spots, which moved and then decayed again.[13]

When considering the main reactions of the intrinsic pathway of coagulation, we constructed the model in which autowave behavior was found[14,15] for the range of reaction parameters observed experimentally. This result is consistent with the hypothesis postulating the two-autowave mechanism of blood coagulation described earlier.[10] In fact, in the model of the intrinsic pathway, we have found one of these two postulated autowaves. Analysis of the mechanisms that can stop the coagulation autowave indicates thrombin switching as the most likely one. In this study, we include this mechanism into the model described previously.[14] The dynamics of this model proved to possess certain properties interesting from the standpoint of the theory of self-organization.

This model predicts a new regime, along with several known wave-propagation regimes found in other models of

a)Electronic mail: fazli@bioscience.msk.su

active media. In the case of one spatial dimension, a pulse runs from the point of activation for a while and then stops. The corresponding spatially nonuniform solution is stationary, and the pulse does not die out. In the two-dimensional case, all active variables also form stationary structures. Note that both active variables have equal diffusion coefficients in this model.

Similar structures were described by Kerner and Osipov.[16] However, the variables they considered had very different diffusion coefficients. The patterns that we have found appear like the ''excitons'' described by Zaikin[17] for a two-dimensional case. Unlike our structures, Zaikin's ''excitons'' exist only when moving. Similar structures were also described by Pearson *et al.*,[18,19] by Krischer and Mikhailov,[20] and later by Schenk *et al.*[21] However, in their model studies,[16,21] the values of diffusion coefficients of the activator and its inhibitor differ significantly, whereas in this study they are set equal. Qualitative analysis of the emergence and evolution of moving spots is usually performed by asymptotic methods. The activator-to-inhibitor diffusion coefficient ratio is chosen as a small parameter in the series expansion procedure. The inhibitor, which diffuses faster, has a broader distribution and constrains the activator spreading. In our model, the inhibitor also exhibits a broader distribution despite the equality of its diffusion coefficient to that of the activator. This broader distribution of the inhibitor seems to be a result of its autocatalytic production.

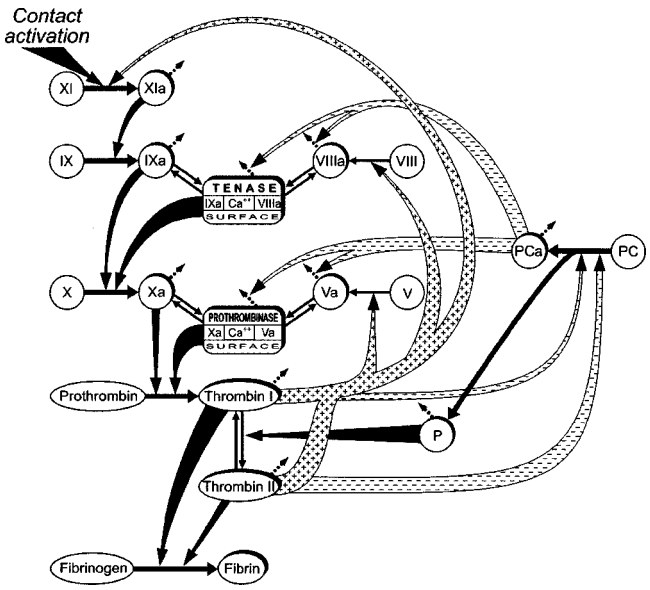

FIG. 1. Scheme of the reaction cascade of blood coagulation forming the basis for mathematical model (2.1)–(2.11). Numbers in circles correspond to different coagulation factors according to their common classification. The same number are used in the mathematical model to designate concentrations of the respective factors. Shadowed circles and index a denote the active forms of the factors; shadowed rectangles are the active complexes with the cofactors. Straight arrows indicate precursors activation; converging arrows—the enzymatic action of active factors and complexes; dashed arrows—the inactivation of active factors by the blood plasma inhibitors (e.g., antithrombin III, a2-macroglobuline, etc.). Hollow arrows with ''+'' symbols are for positive feedback reactions, while those with ''−'' symbols are for negative feedback reactions.

II. DESCRIPTION OF THE MATHEMATICAL MODEL

The key clotting enzyme thrombin is generated by the cascade of proteolytic reactions and catalyzes the formation of fibrin. Fibrin polymerization leads to the appearance of a clot. Several positive feedback loops arises from thrombin, resulting in its self-accelerated production. The threshold properties of blood clotting and the autowave nature of thrombin expansion are the consequences of these kinetic characteristics of thrombin generation. If thrombin expands as an autowave, the question of how the clot stops growing becomes of primary importance. In Refs. 10 and 11 we speculated that clot growth is terminated because active thrombin can produce its own inhibitor in a self-accelerated manner. In fact, thrombin activates protein *C*, which is one of the most important factors that abrogate thrombin generation. However, experimental evidence for autocatalytic protein *C* production (the presence of positive feedback loops in the protein *C* activation pathway) is still lacking. On the other hand, the data have been reported, indicating that thrombin can exist in two states—procoagulant and anticoagulant.[22,23] In the procoagulant state the rate constant for thrombin interaction with fibrinogen is high, while the rate constant for its interaction with protein *C* is low. Conversely, in the anticoagulant state thrombin is more active towards protein *C* than towards fibrinogen.

In this study, the model developed previously to describe the spatial dynamics of blood clotting[14,15] was extended to include reactions of switching thrombin between its procoagulant and anticoagulant states. We now hypothesize that switching between thrombin's states is a physiological mechanism involved the termination of clot growth. The model is based on the scheme of molecular processes shown in Fig. 1. Coagulation factors are given in common designations. Subscript ''a'' marks the activated form of the factor. The initiation of clotting leads to the assembly of prothrombinase, which produces thrombin in the procoagulant state (*Thrombin I*), in which it rapidly converts fibrinogen into fibrin and slowly activates protein *C* (Fig. 1). Activated protein *C* proteolytically destroys cofactors *Va* and *VIIIa*. It is conceivable that one of the products of these reactions (product *P* in Fig. 1) can act as an effector that switches *Thrombin I* into its anticoagulant state (*Thrombin II*). Upon switching, the cleavage rate of fibrinogen decreases, whereas the rate of protein *C* activation and, therefore, the rate of the effector accumulation increase. This, in turn, stimulates the transition of thrombin into its anticoagulant state and leads to the self-accelerated inhibition of clot growth. At present, the molecular identity of such effector is not known. The nature of the effector is not so important for mathematical study. Thus, we assume that this effector (product *P* in Fig. 1) is a product of protein *C* cleavage by thrombin. In this model, both thrombin forms are equally active toward other thrombin substrates, such as factors *XI*, *V*, and *VIII*. In the previous model,[14,15] the dynamics of thrombin was described by only one equation. In this model, the procoagulant and anticoagulant forms of thrombin are considered separately. In fact, the revision concerns only the equations for protein *C* and fibrin.

The mathematical model corresponding to scheme 1 is

the following set of parabolic-type partial differential equations:

$$\frac{\partial XIa}{\partial t}=k_{11}(IIa_1+IIa_2)-h_{11}XIa+D\Delta XIa, \tag{2.1}$$

$$\frac{\partial IXa}{\partial t}=k_9XIa-h_9IXa+D\Delta IXa, \tag{2.2}$$

$$\frac{\partial Xa}{\partial t}=k_{10}IXa+\overline{k_{10}}Z-h_{10}Xa+D\Delta Xa, \tag{2.3}$$

$$\frac{\partial IIa_1}{\partial t}=k_2Xa\frac{II}{(II+K_{2m})}+\overline{k_2W}\frac{II}{(II+\overline{K_{2m}})}=h_2IIa_1 - k'IIa_1P+k''IIa_2+D\Delta IIa_1, \tag{2.4}$$

$$\frac{\partial IIa_2}{\partial t}=-h_2IIa_2+k'IIa_1P-k''IIa_2+D\Delta IIa_2, \tag{2.5}$$

$$\frac{\partial II}{\partial t}=-k_2Xa\frac{II}{(II+K_{2m})}-\overline{k_2W}\frac{II}{(II+\overline{K_{2m}})}+D\Delta Pt, \tag{2.6}$$

$$\frac{\partial P}{\partial t}=k_{apc1}IIa_1+k_{apc2}IIa_2-h_pP+D\Delta P, \tag{2.7}$$

$$\frac{\partial VIIIa}{\partial t}=k_8(IIa_1+IIa_2)-k_aPCa(VIIIa+Z) - h_8VIIIa+D\Delta VIIIa, \tag{2.8}$$

$$\frac{\partial Va}{\partial t}=k_5(IIa_1+IIa_2)-k_aPCa(Va+W)-h_5Va + D\Delta Va, \tag{2.9}$$

$$\frac{\partial PCa}{\partial t}=k_{apc1}IIa_1+k_{apc2}IIa_2-h_{apc}PCa+D\Delta PCa, \tag{2.10}$$

$$\frac{dIa}{dt}=k_{1,1}IIa_1+k_{1,2}IIa_2. \tag{2.11}$$

The model variables are the concentrations of factors *XIa*, *IXa*, *Xa*, IIa_1 (*Thrombin I*), IIa_2 (*Thrombin II*), *II* (prothrombin), *P* (peptide *P* in Fig. 1), *VIIIa*, *Va*, *Z* (tenase), *W* (prothrombinase), *PCa* (activated protein *C*), and *Ia* (fibrin); k_i is the product of the rate constant and the concentration of the nonactivated *i*th factor for (2.1)–(2.3), (2.6)–(2.11); and h_i is the rate constant for inactivation of the *i*th factor by plasma inhibitors. *Thrombin I* generation [see Eq. (2.4)] obeys the Michaelis–Menten kinetics. Here we use the designations introduced previously.[14,15]

We assume that the assembly of both tenase and prothrombinase are stationary processes. The quasistationary concentrations of tenase and prothrombinase complexes appear as[14]

$$W=\frac{k_{510}XaVa}{(h_{510}+k_aPCa)}, \quad Z=\frac{k_{89}IXaVIIIa}{(h_{89}+k_aPCa)}.$$

The following assumptions were made concerning the rate constants for thrombin interaction with its putative effector *P*. We propose that they bind fastly and that a dynamic equilibrium exists between the two thrombin forms. The effector *P* concentration determines this equilibrium. This assumption is based on the fact that the rate constants for thrombin binding with low-molecular-weight effectors are usually quite high.[24]

Therefore, it is reasonable to assume that $h_2 \ll k''$. If so, $IIa_2=(k'/k'')\,IIa_1P$. Let (k''/k') be equal to k_p. From $IIa=IIa_1+IIa_2$ we obtain $IIa_1=k_pIIa/(k_p+P)$ and $IIa_2=PIIa/(k_p+P)$. Considering the peptide *P* concentration to be quasistationary, we can set the right-hand part of Eq. (2.7) to zero. Solving this equation, we find

$$P=\frac{(k_{apc2}IIa-h_pk_p)+\sqrt{(k_{apc2}IIa-h_pk_p)^2+4k_{apc1}k_ph_pIIa}}{2h_p}. \tag{2.12}$$

Note that $(dIIa/dt)=(dIIa_1/dt)+(dIIa_2/dt)$. These assumptions allow us to simplify the model as follows:

$$\frac{\partial XIa}{\partial t}=k_{11}IIa-h_{11}XIa+D\Delta XIa, \tag{2.13}$$

$$\frac{\partial IXa}{\partial t}=k_9XIa-h_9IXa+D\Delta IXa, \tag{2.14}$$

$$\frac{\partial Xa}{\partial t}=k_{10}IXa+\overline{k_{10}}\frac{k_{89}IXaVIIIa}{(h_{89}+k_aPCa)} - h_{10}Xa+D\Delta Xa, \tag{2.15}$$

$$\frac{\partial IIa}{\partial t}=k_2Xa\frac{II}{(II+K_{2m})} +\overline{k_2}\frac{k_{510}XaVa}{(h_{510}+k_aPCa)}\frac{II}{(II+\overline{K_{2m}})} - h_2IIa+D\Delta IIa, \tag{2.16}$$

$$\frac{\partial II}{\partial t}=-k_2Xa\frac{II}{(II+K_{2m})} -\overline{k_2}\frac{k_{510}XaVa}{(h_{510}+k_aPCa)}\frac{II}{(II+\overline{K_{2m}})}+D\Delta II, \tag{2.17}$$

$$\frac{\partial VIIIa}{\partial t} = k_8 IIa - k_a PCa\left(VIIIa + \frac{k_{89} IXa VIIIa}{(h_{89} + k_a PCa)} \right) - h_8 VIIIa + D\Delta VIIIa, \tag{2.18}$$

$$\frac{\partial Va}{\partial t} = k_5 IIa - k_a PCa\left(Va + \frac{k_{510} Xa Va}{(h_{510} + k_a PCa)} \right) - h_5 Va + D\Delta Va, \tag{2.19}$$

$$\frac{\partial PCa}{\partial t} = \frac{(k_{apc1} k_p + k_{apc2} P)}{(k_p + P)} IIa - h_{apc} PCa + D\Delta PCa, \tag{2.20}$$

$$\frac{dIa}{dt} = \frac{(k_{1,1} k_p + k_{1,2} P)}{(k_p + P)} IIa, \tag{2.21}$$

where

$$P = \frac{(k_{apc2} IIa - h_p k_p) + \sqrt{(k_{apc2} IIa - h_p k_p)^2 + 4 k_{apc1} k_p h_p IIa}}{2 h_p},$$

$IIa = IIa_1 + IIa_2$ (the sum of both forms of thrombin).

The model variables are the concentrations of factors *XIa*, *IXa*, *Xa*, *IIa* (thrombin), *II* (prothrombin), *VIIIa*, *Va*, *PCa* (activated protein *C*), and *Ia* (fibrin). The rate constants were estimated from the available experimental data (for the procedure of estimating the constants from experimental data see Ref. 14). The constant for equilibrium between the two thrombin forms (k_p) was assumed to be on the order of the rate constant for assembly of tenase and prothrombinase complexes. We set it to 10 nM. As the rate constants for coagulation factor inactivation are usually several tenths of minutes^{-1}, we assumed the rate constant for peptide *P* inactivation (h_p) to be 1 min^{-1}. The rate constant for protein *C* activation by the second form of thrombin (k_{apc2}) was varied from 0.0014 min^{-1} (known from the literature for k_{apc1}) to the values several orders of magnitude higher in an attempt to increase the efficiency of switching.

Introducing the mechanism for switching thrombin between its two forms into the model almost does not alter the homogeneous kinetics of coagulation. Therefore, model (2.13)–(2.21) is similar to the original model[14,15] in describing the experimental data on the homogeneous kinetics. Both models quantitatively describe the characteristic time required for the blood activated via the intrinsic pathway to coagulate, the peak thrombin concentration for a given activation level and the activation threshold. Model (2.13)–(2.21) also describes quantitatively the dynamics of clot growth, observed in experiments[11] (the lag time and the rate in the linear range of growth) for the set of rate constants shown in Table I.

In this case, the thrombin autowave propagates from the point of activation with practically constant velocity and then abruptly stops. Along with these solutions, more complicated behavior and spatiotemporal structures can be found in the model.

We simplified the model to qualitatively study its dynamics. The variables *IXa*, *Xa*, *Va*, and *VIIIa* were considered to be fast. Therefore, Eqs. (2.14), (2.15), (2.18), and (2.19) were replaced by the corresponding algebraic (steady-state) expressions. As the rates of production of these factors are known to be high, we assumed their spatial concentrations to be constant and close to equilibrium ones. Instead of Eq. (2.17), a limit on the maximum value of thrombin (*Pt0*) was introduced into the equation for thrombin generation.

TABLE I. Parameter values used in model (2.13)–(2.21) to describe the experimentally observed dependence of the clot size on time [Fig. 5(c) p. 460 in Ref. 11]. Specifically, a quasi-one-dimensional problem with cylindrical symmetry $\{\Delta = (1/r)(\partial/\partial r)[r(\partial/\partial r)]\}$ was solved for the following boundary conditions: $D(\partial XIa/\partial r)|_{r=r0} = A$, $D(\partial XIa/\partial r)|_{r=R} = 0$, $D(\partial F_i/\partial r)|_{r=R}^{r=r0} = 0$, where $r0$ ($r0 = 0.25$ mm) is the radius of the activating glass bead, $D = 3.7\times10^{-3}$ mm^2 min^{-1}, $A = 5\times10^{-3}$ mm nM min^{-1}, and F_i denotes the coagulation factor *IXa*, *Xa*, *IIa*, *II*, *VIIIa*, *Va*, or *APC*.

k_{11}	h_{11}	k_9	h_9	k_{10}	$\overline{k_{10}}$	k_8	h_8
0.000011 min^{-1}	0.2 min^{-1}	20 min^{-1}	0.2 min^{-1}	0.0033 min^{-1}	500 min^{-1}	0.000 01 min^{-1}	0.31 min^{-1}
k_a	k_5	h_5	h_{10}	h_2	k_2	$\overline{k_2}$	h_p
1.2 min^{-1} nM^{-1}	0.17 min^{-1}	0.31 min^{-1}	1 min^{-1}	2.3 min^{-1}	2.45 min^{-1}	2000 min^{-1}	1 min^{-1}
k_{89}	h_{89}	k_{510}	h_{510}	k_{apc1}	k_{apc2}	k_p	h_{apc}
100 min^{-1} nM^{-1}	100 min^{-1}	100 min^{-1} nM^{-1}	100 min^{-1}	0.0014 min^{-1}	0.07 min^{-1}	10 nM	0.1 min^{-1}

TABLE II. A set of parameters with which a stationary standing structure arises in model (2.22) as a solution to the one-dimensional problem [$\Delta=(\partial^2/\partial x^2)$]. Diffusion flux was set to zero at the ends of the straight-line segment. Activation of the system was modeled as a local rise in the first variable at the left boundary. The diffusion coefficient D was set to 6×10^{-4} mm^2 min^{-1}. Asterisks indicate the constants that differ from the respective constants in Table I.

k_{11}^*	h_{11}	k_9	h_9	k_{10}	$\overline{k_{10}}$	k_8	h_8^*
0.0001 min^{-1}	0.2 min^{-1}	20 min^{-1}	0.2 min^{-1}	0.0033 min^{-1}	500 min^{-1}	0.000 01 min^{-1}	137 min^{-1}
k_a	k_5	h_5	h_{10}	h_2	k_2	$\overline{k_2}$	h_p
1.2 min^{-1} nM^{-1}	0.17 min^{-1}	0.31 min^{-1}	1 min^{-1}	2.3 min^{-1}	2.45 min^{-1}	2000 min^{-1}	1 min^{-1}
k_{89}	h_{89}	k_{510}	h_{510}	k_{apc1}	k_{apc2}^*	k_p^*	h_{apc}^*
100 min^{-1} nM^{-1}	100 min^{-1}	100 min^{-1} nM^{-1}	100 min^{-1}	0.0014 min^{-1}	0.0208 min^{-1}	5 nM	0.143 min^{-1}

Because fibrin does not influence the kinetics of other coagulation factors Eq. (2.21) was excluded. Therefore, the set of Eqs. (2.13)–(2.21) was reduced to the following system:

$$\begin{aligned}
\frac{\partial IIa}{\partial t} &= D\Delta IIa + \frac{k_9}{h_9 h_{10}} XIa\left(k_{10}+\overline{k_{10}}k_8\frac{k_{89}}{h_{89}}\frac{IIa}{(h_8+k_aPCa)}\right)\\
&\quad\times\left(k_2+\overline{k_2}k_5\frac{k_{510}}{h_{510}}\frac{IIa}{(h_5+k_aPCa)}\right)\\
&\quad\times\left(1-\frac{IIa}{Pt0}\right)-h_2IIa,\\
\frac{\partial XIa}{\partial t} &= D\Delta XIa + k_{11}IIa - h_{11}XIa,\\
\frac{\partial PCa}{\partial t} &= D\Delta PCa + \frac{(k_{apc1}k_p+k_{apc2}P)}{(k_p+P)}IIa - h_{apc}PCa,
\end{aligned} \tag{2.22}$$

$$P=\frac{(k_{apc2}IIa-h_pk_p)+\sqrt{(k_{apc2}IIa-h_pk_p)^2+4k_{apc1}k_ph_pIIa}}{2h_p}.$$

All designations in (2.22) are the same as in Eqs. (2.13)–(2.21).

In this reduced model, a parameter range can be found where a solitary stationary standing structure arises. In our opinion, its existence is the most intriguing regime in this model (one set of parameters from this range is shown in Table II).

When this set of parameters is used in model (2.13)–(2.21), a thrombin peak located at some distance from the point of activation persists for a long time, until prothrombin is depleted.

Using characteristic values of the variables [$IIa=X_0u_1$, $XIa=Y_0u_2$, $PCa=Z_0u_3$, $t=T_0\tilde{t}$, $X_0=Pt0$, $Y_0=(k_{11}X_0/h_2)$, $Z_0=(X_0k_{apc1}/h_2)$, and $T_0=(1/h_2)$], we can rewrite the equations in the dimensionless form

$$\begin{aligned}
\frac{\partial u_1}{\partial\tilde{t}} &= D\Delta u_1 + M_1(1-u_1)u_2\left[1+\frac{M_2u_1}{(1+M_3u_3)}\right]\\
&\quad\times\left[1+\frac{M_4u_1}{(1+M_5u_3)}\right]-u_1,\\
\frac{\partial u_2}{\partial\tilde{t}} &= D\Delta u_2 + u_1 - M_6u_2,\\
\frac{\partial u_3}{\partial\tilde{t}} &= D\Delta u_3 + \frac{(1+M_7P)}{(1+M_8P)}u_1 - M_9u_3,\\
P &= (u_1-M_{10})+\sqrt{(u_1-M_{10})^2+M_{11}u_1},
\end{aligned} \tag{2.23}$$

$$M_1=\frac{k_{11}k_9k_{10}k_2}{h_2^2h_9h_{10}},\quad M_2=\frac{\overline{k_{10}}k_{89}k_8}{k_{10}h_{89}h_8}X_0,$$

$$M_3=\frac{k_aX_0k_{apc1}}{h_2h_8},\quad M_4=\frac{\overline{k_2}k_{510}k_5}{k_2h_{510}h_5}X_0,$$

$$M_5=\frac{k_aX_0k_{apc1}}{h_2h_5},\quad M_6=\frac{h_{11}}{h_2},\quad M_7=\frac{k_{apc2}^2X_0}{2k_{apc1}k_ph_p},$$

$$M_8=\frac{k_{apc2}X_0}{2k_ph_p},\quad M_9=\frac{h_{apc}}{h_2},\quad M_{10}=\frac{k_ph_p}{X_0k_{apc2}},$$

$$M_{11}=\frac{4k_ph_pk_{apc1}}{X_0k_{apc2}^2}.$$

These equations may be further simplified by neglecting the terms in the first equation that appeared to be small from analysis of the values of rate constants

$$\frac{\partial u_1}{\partial t}=D\Delta u_1+M_1M_4(1-u_1)u_1u_2\frac{(1+M_2u_1)}{(1+M_5u_3)}-u_1. \tag{2.24}$$

It is also possible to modify the third equation without disturbing the shape of the nullclines in the (u_1,u_3) coordinates for the stationary-structure regime.

The resulting set of equations is

$$\frac{\partial u_1}{\partial t} = D\Delta u_1 + K_1 u_1 u_2 (1-u_1)\frac{(1+K_2 u_1)}{(1+K_3 u_3)} - u_1,$$
$$\frac{\partial u_2}{\partial t} = D\Delta u_2 + u_1 - K_4 u_2, \tag{2.25}$$
$$\frac{\partial u_3}{\partial t} = D\Delta u_3 + K_5 u_1^2 - K_6 u_3.$$

By its construction, model (2.25) retains many qualitative properties of the initial system (2.13)–(2.21) describing the clotting cascade; therefore, later, we will analyze only model (2.25).

III. COMPUTER SIMULATIONS

System (2.25) was solved numerically. We used Numerov's approximation of the fourth order for spatial terms.[25] Each set of differential equations was discretized in space and solved by the Runge–Kutta–Felberg method of the 2(3) order.[25] Note that, by construction, the resulting difference scheme is similar to the so-called ''compact schemes,'' which are successfully used to solve numerically fluid dynamic problems.[26] In the one-dimensional case, we used no-flux boundary conditions: diffusion flux was set to zero at the ends of the straight-line segment.

The difference scheme was analyzed for stability in a linear approximation. To this end, we wrote the corresponding variational equations and examined them using the von Neumann method. In this way, the difference scheme employing an variable time step size was proven to be stable. An additional requirement that perturbations propagate along the grid at the same characteristic rate as in the differential problem, leads to the following condition:

$$h < 2\sqrt{\frac{D}{a_-}\left(\sqrt{\frac{a_+}{a_-}} - \sqrt{\frac{a_+}{a_-} - 1}\right)}, \tag{3.1}$$

where D is the diffusion coefficient; a_+ and a_- are the greatest and the smallest real parts, respectively, of the eigenvalues of the Jacobi matrix, which corresponds to the solution to the reaction part of the set under consideration. Estimates for a_+ and a_- are the respective real parts calculated along the solution to the spatially homogeneous problem. In Sec. IV B, the spatial step was selected to met (3.1): $h = 0.001$.

Interactive local bifurcation analyzer (LocBif)[27] software was used to construct bifurcation diagrams.

IV. RESULTS

A. Behavior of the system with full stirring

Let us consider the spatially homogeneous system corresponding to (2.25) and analyze its equilibrium states. The roots of the following polynomial (4.1) determine the stationary points of model (2.25):

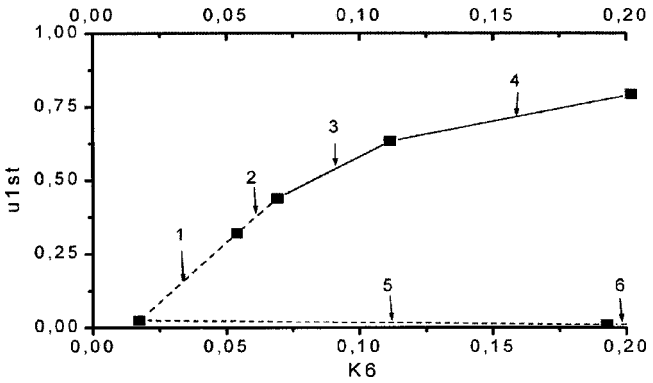

FIG. 2. Bifurcation diagram u_{1st} (steady-state concentration of thrombin) vs parameter K_6 for model (2.25). Solid and dotted lines denote stable and unstable states, respectively; $K_6 = 0.0692$ corresponds to Poincare–Andronov–Hopf bifurcation. Other parameter values are specified in Table III for $D = 0$. Stationary points are indicated by numbers: (1, 5) unstable saddle-node, (2, 6) unstable focus, (3) stable focus, and (4) stable node.

$$f(u_1) = u_1\left\{\frac{K_1 K_2}{K_4}u_1^3 + \left[\frac{K_1}{K_4}(1-K_2) + \frac{K_3 K_5}{K_6}\right]u_1^2 - \frac{K_1}{K_4}u_1 + 1\right\}. \tag{4.1}$$

The system always contains the trivial (zero) stationary point, which is stable for any parameter values. In addition, polynomial (4.1) always possesses one negative root. Depending on the parameters of the model the number of its positive roots, which determine the stationary points of model (2.25), may vary from 0 to 2.

It is convenient to analyze the model behavior by varying the parameter K_2, which characterizes the activator production rate, and the parameter K_6, which sets the inactivation rate for the inhibitor. Figure 2 shows the bifurcation diagram computed with K_6 ranging from 0 to 0.2 and the other parameters fixed (see Table III). The coordinates of the stationary points for the first variable are plotted as ordinates [its relationships with the other variables are given by the expressions $u_{2st} = (u_{1st}/K_4)$ and $u_{3st} = (K_5/K_6)\,u_{1st}^2$]. The solid and dashed lines correspond to the stable and unstable stationary states, respectively.

For $K_6 = 0.0173$, zero is a unique stationary point in the system. Two more equilibrium points emerge at $K_6 > 0.0173$. The two curves that arise from the point $K_6 = 0.0173$ show the evolution of the coordinate u_1 of these stationary points upon varying parameter K_6. The stationary point corresponding to the lower branch (of the saddle-node type for $K_6 < 0.193$ or the saddle-focus type if $K_6 > 0.193$) is unstable. As K_6 increases, the value of u_{1st} decreases. The second stationary point, which is unstable at low K_6, be-

TABLE III. Model parameters used for numerical calculations.

K_1	K_2	K_3	K_4	K_5
6.85	11.0	2.36	0.087	17.0

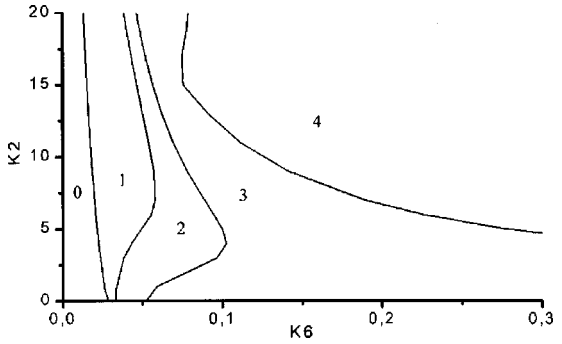

FIG. 3. The evolution of the type of the stationary point farthest relative to the origin. Other constants are specified in Table III for $D=0$.

comes stable at $K_6=0.0692$. The Poincare–Andronov–Hopf (PAH) bifurcation corresponds to this value of the parameter.

Figure 3 illustrates the evolution of the type of the farthest stationary point (relative to the origin) in the $(K_2;K_6)$ parameter plane. Regions 1–4 are numbered according to the type of the stationary point under consideration (see Fig. 2). The stationary point is unstable in regions 1 and 2 and stable in regions 3 and 4. In region 0 (positive quadrant), zero is the only stationary point of model (2.25). Region 2 expands as K_2 decreases. Numerical experiments have revealed a cascade of period-doubling bifurcations in this region and a transition to chaotic oscillations by the Feigenbaum scenario. If the other parameters have values indicated in Table III, limit cycles and chaos exist in a very narrow range of K_6 values, which is adjacent to the PAH bifurcation line at the left. The chaotic attractor structure and the problem of chemical turbulence emergence in distributed systems are remained to be explored in further publications. In this study, we address first and foremost the issues of spatial pattern formation.

B. Spatial dynamics of model (2.25)

The one-dimensional problem was considered in the segment of length $L=10$ ($\Delta=\partial^2/\partial x^2$). The diffusion coefficients of all model variables were assumed to be equal: $D=0.000\,26$. Activation of the system was modeled as a local rise in the first variable at the left boundary (specifically, u_1 was set to 0.5 at 30 points adjacent to the left boundary).

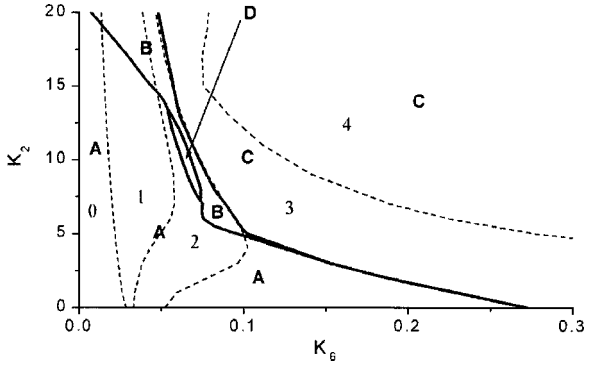

FIG. 4. Zones of different types of thrombin propagation in the K_2–K_6 parameter plane. See Table III for other parameters. Dotted lines are the boundaries indicated in Fig. 3 by solid lines.

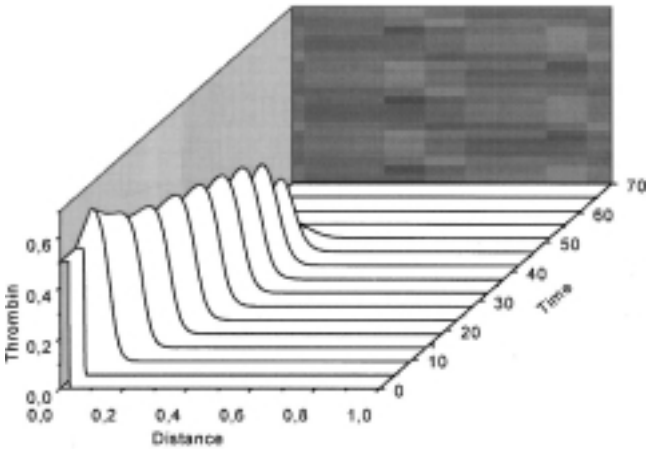

FIG. 5. Thrombin pulse (u_1) propagating (region A in Fig. 4) with decreasing amplitude and speed: $K_2=11.0$, $K_6=0.055$; for other constants see Table III.

Figure 4 shows the bifurcation diagram of the spatially distributed system in the $(K_2;K_6)$ parameter plane. Solid lines stand for the boundaries between the different modes of perturbation propagation. Dashed lines correspond to bifurcations of the homogeneous solution to system (2.25) shown in Fig. 3. All the regimes of model behavior detected in this study can be divided into four types (A–D in Fig. 4), each of them we consider later.

1. Region A

In the region corresponding to regime A, the initial perturbation is damped, and the system settles down to the trivial spatially homogeneous solution. Figure 5 shows the evolution of the initial perturbation for $K_2=11.0$ and $K_6=0.055$, lying in this region (see the Table III for the values of other constants). A pulse is slowed down and its amplitude diminishes; eventually, the pulse disappears completely. When comparing Figs. 6 and 3, we see that, for $K_2<14$, the parameter range in which perturbations are damped includes entire regions 0 and 1 (Fig. 3) and a large portion of region 2. In this range, the only stable point existing in the homogeneous system is zero. If $K_2<5$, region A includes part of

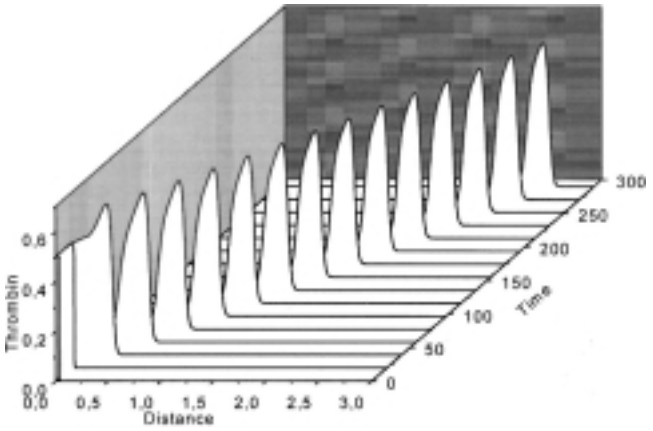

FIG. 6. Self-sustained propagation of a thrombin pulse for $K_2=14.0$, $K_6=0.061$ (region B in Fig. 4); other constants are specified in Table III.

region 3, in which the corresponding homogeneous system possesses an additional nontrivial stable stationary point, and, hence, exhibits bistability. Therefore, the system may be found turns out to be in the basin of attraction of any of the two stationary points; its position will depend on the selection of initial conditions. Under the initial conditions specified above ($u_1=0.5$ at 30 points), the system is in the basin of attraction of the trivial steady state, and the initial perturbations are damped. To bring the system into the basin of attraction of the second point and to initiate a trigger wave, we have to enlarge the area of the initial perturbation while decreasing its amplitude (e.g., to set u_1 to be 0.3 at 200 points). This makes it possible to overcome the threshold that exists in the spatially distributed system. The presence of this type threshold in trigger-type systems was acknowledged for Ref. 28.

2. Region B

If K_2 leaves region A, a running pulse is observed in the system; the pulse propagates without attenuation (Fig. 6). This area, corresponding to the autowave regime, includes the upper portions of ''strips'' 0 and 1 (see Fig. 4) and almost entirely the part of region 2 adjacent to its right boundary. An increase in K_2 and K_6, especially in K_2, results in stabilizing the autowave pattern. At $K_2<5$, the solution exhibits a complicated dependence on the initial condition, and a transition to regimes of turbulence is observed. In this range, chaotic spatial oscillations (or chemical turbulence) may arise.[29] We also have found a pulse, which propagates with oscillating amplitude (Fig. 7). This regime imitates the stratified structure previously observed experimentally.[11]

3. Region C

The right boundary of region B fairly well coincides with the PAH bifurcation line for $K_2>5$ (Fig. 4). To the right from this boundary, in region C, a trigger wave is generated in response to perturbation (Fig. 8). It corresponds to the regime of bistability, in which the respective homogeneous system possesses two stable stationary points.

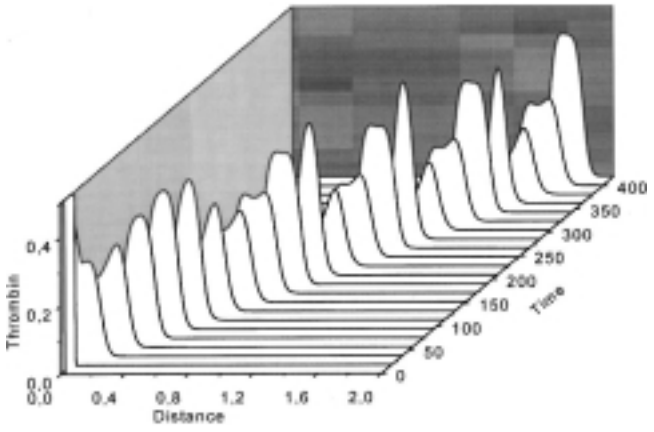

FIG. 7. Thrombin wave with oscillating amplitude for $K_2=6.5$, $K_6=0.075$ (region B in Fig. 4); for other constants see Table III. Such propagation imitates the formation of stratified structures.

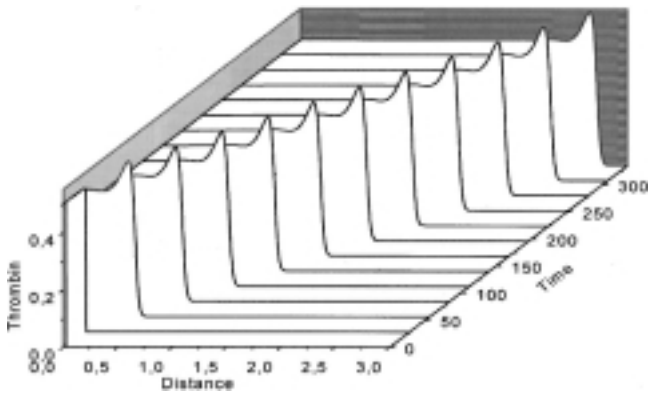

FIG. 8. Trigger wave propagation in the region of bistability (region C in Fig. 4). Calculations were performed for $K_2=11.0$ and $K_6=0.069$; the other parameters are shown in Table III.

4. Region D

In a certain range of K_2 values corresponding to a transition from attenuation of the initial perturbation (region A) to the regime of running pulses (region B), there exists region D, in which an unusual regime has been detected: a pulse running from the activation zone stops but does not died out; rather, it is stabilized and exists indefinitely long (Fig. 9). This solution was studied analytically and proven to be an actual steady state of the system (see Appendix A). Analysis of this solution for stability is given in Appendix B. Figure 10 shows the spatial distributions of all variables in the steady-state structure, whose parameters are specified in Fig. 9. Each curve was normalized to its maximum. Compared with u_1 (activator), u_3 (inhibitor), and u_2 exhibited broader distributions. This ensured the formation of the stationary structure. To clarify whether the patterns do exist and whether the difference scheme used converges, we have carried out a series of computations, varying the spatial step h. Neither the region D characteristics (size, form, location), nor the process of pattern generation changed upon varying h below 0.005. Analytical estimation of the spatial step optimum, based on minimization of the approximation error of the method and the round-off errors, leads to the h value of about 0.001. The segment over which integration is performed must be several times longer than the characteristic size of the developing structure, in order to prevent the po-

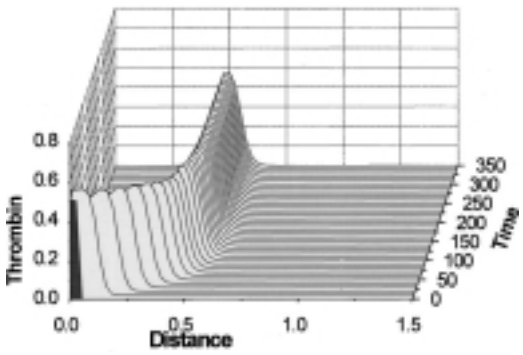

FIG. 9. Standing nonuniform pattern formation for $K_2=11.0$, $K_6=0.062$, and other constants as indicated in Table III (region D in Fig. 4).

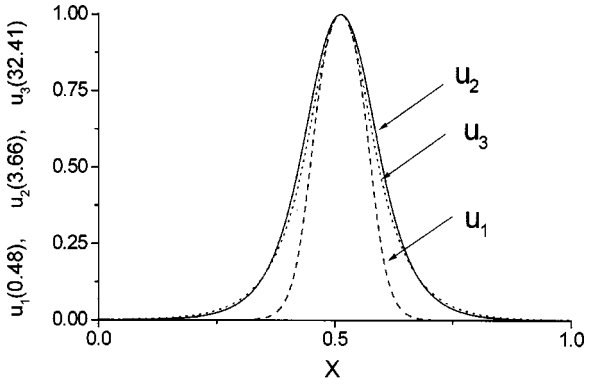

FIG. 10. Spatial distribution of variables u_1, u_2, and u_3 in the stationary pattern normalized to their respective maxima (which are indicated in parentheses).

tential effect of the boundary conditions on the process of patterning. In the region D, model behavior does not depend qualitatively on the activation mode. The initial conditions determine only the distance from the site of activation at which the structure is generated.

Figures 11(a) and 11(b) show how the amplitude of the standing pattern formed and the distance from the activating boundary change with increasing K_6 (if other computation parameters, such as length of the segment for integration, step h, and initial conditions, are kept fixed). Evidently, an increase in K_6 only slightly raises the amplitude of the developing pulse. However, the distance at which the pulse

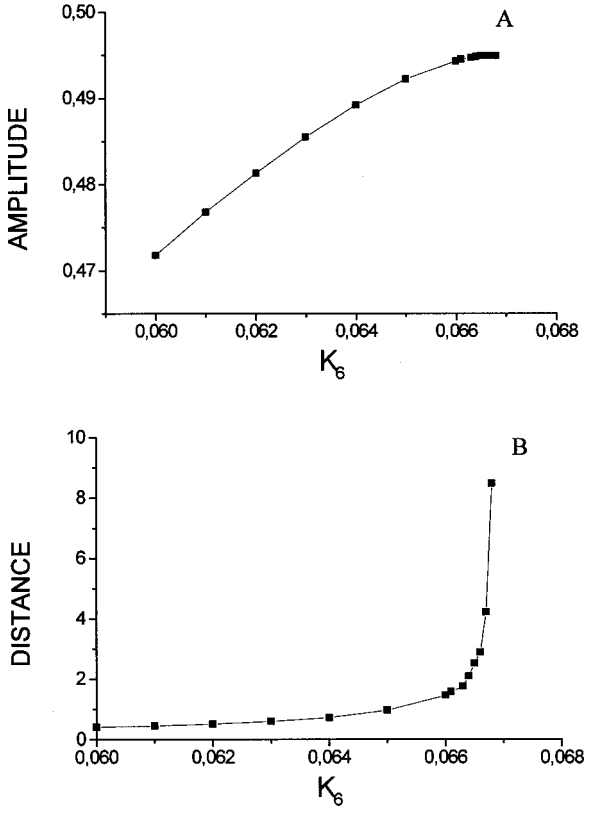

FIG. 11. Changes (a) in the amplitude of variable u_1 for the standing pattern and (b) its distance from the activating boundary with increasing K_6 within region D for $K_2=11.0$. For other constants see Table III.

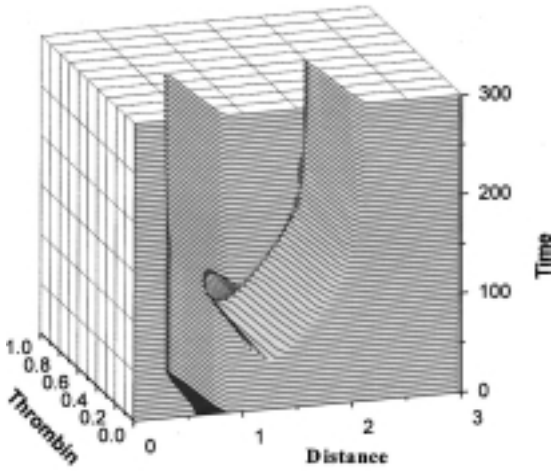

FIG. 12. Interaction between the moving and stationary pulses. In simulations $K_2=12.0$, $K_6=0.59$, and all other constants are as indicated in Table III. The perturbation was placed in the vicinity of the stationary motionless structure at $t=50$, leading to a formation of two pulses moving away from each other. The impulse moving leftwards towards the stationary structure ''collides'' with it and decays quickly, while the impulse moving in the opposite direction forms a motionless structure.

stops running steeply increases with increasing K_6, tending to infinity. This causes a transition into region B, corresponding to running pulses.

For region D we also performed analysis of a ''collision'' between a running pulse tending to its stationary solution, and a motionless pulse structure that has already reached its steady state (Fig. 12). The standard perturbation was introduced in the vicinity of the motionless stationary structure at $t=50$ (see Methods). This perturbation leads to a formation of two pulses moving in opposite directions. Normally, in isotropic medium these pulses stop at some distance from the point of their origin and exist as motionless stationary structures. However, when such impulses are born in the vicinity of another stationary structure, the impulse that moves towards this structure dissipates at some distance from it. Coincidentally, the stationary pulse is perturbed but then relaxes to the state with initial amplitude. The pulse moving rightwards, i.e., away from the stationary structure (Fig. 12), gives rise to a normal stationary, motionless structure. The stability of the resulting pattern is considered for the one-dimensional case in Appendix B.

V. DISCUSSION

In the model examined, we observed the formation of a solitary stationary structure. The mechanism whereby it arises is essentially different from the known mechanisms of pattern formation.[1–9] Our theoretical model (2.25) is significantly different from the well-known basic models of spontaneous pattern formation and self-organization in nonequilibrium systems of different natures.[1–9] Solitary spots (both moving and stationary) were analyzed by Kerner and Osipov. The most comprehensive description of these structures called autosolitons is given in Ref. 16. The spatially localized structures in homogeneous dissipative two-component systems, described by Kerner and Osipov, are characterized by different diffusion coefficients of the activator and its in-

hibitor. Along with the classic case of Turing instability, they considered a situation with the short-range inhibitor and long-range activator.

The mechanism of patterning described in the present study is distinct from the mechanism whereby stationary lamellar patterns are generated in chemical systems.[6] In the latter, the initial and growing structures are topologically equivalent at every point in time, while the structure formation by the biwave mechanism occurs through successively adding structural elements to those formed earlier. Finally, our model differs from those studied in the theory of biological pattern formation[4,5] mainly because the latter has a single autocatalytic variable. We also suggest that autowave mechanisms similar to that proposed for blood clotting may be involved in a step-by-step pattern formation during biological developmental processes.

The relationship between the topological properties of slow manifolds of the chemical system (catastrophes) and the type of wave or pulse propagation has been considered in studies[30,31] by Ortoleva. Unlike his models, our model is constructed without the use of slow manifold formalism in the explicit form.

It seems likely that nature uses such self-organizing principles not only in blood coagulation, but also in other biological systems. Spatial differentiation phenomena in multicellular organisms share many features in common with the process of clot formation. In the hypothesis proposed, biochemical aspects of the problem are considered in detail. We discuss the mechanisms controlling the spatiotemporal organization of coagulation. Its metabolic basis is the enzymatic cascade. Cascades of phosphokinases and proteases are common in biology. For many of them, control mechanisms are not known as yet. It is conceivable that all these cascades, blood coagulation included, are regulated in a similar manner.

ACKNOWLEDGMENTS

The authors thank Dr. A. M. Zhabotinsky and Dr. A. Loskutov for critically reading the manuscript, Dr. R. I. Volkova for her useful comments and help, and A. Yu. Kondratovich for technical assistance. This study was supported in part by the Russian Foundation for Basic Research (Projects Nos. 97-04-49223 and 00-04-48855) and by the Russian Ministry of Science (No. A76).

APPENDIX A: STABILITY ANALYSIS OF THE STATIONARY SPATIALLY NONUNIFORM SOLUTION

Let us rewrite the set (2.25) in a form convenient for analysis of stability of the stationary spatially nonuniform solution

$$\begin{aligned}
&\frac{\partial u_1}{\partial t} - D u_{1xx}'' + u_1 + f_1(u_1,u_2,u_3) = 0,\\
&\frac{\partial u_2}{\partial t} - D u_{2xx}'' - u_1 + K_4 u_2 = 0,\\
&\frac{\partial u_3}{\partial t} - D u_{3xx}'' + K_6 u_3 + f_3(u_1) = 0.
\end{aligned} \tag{A1}$$

Here, f_1, f_3 denote nonlinear terms of the corresponding equations

$$f_1 = -K_1(1-u_1)u_1u_2\frac{(1+K_2u_1)}{(1+K_3u_3)},$$

$$f_3 = -K_5u_1^2.$$

Let the boundary conditions be as follows:

$$\left.\frac{\partial u_i}{\partial x}\right|_{\substack{x=0\\x=L}} = 0, \quad i = 1,2,3.$$

In a vector form, set (A1) is

$$\left(\frac{\partial}{\partial t} - \hat{D}\frac{\partial^2}{\partial x^2} + A\right)\mathbf{u} + \mathbf{f}(\mathbf{u}) = 0, \tag{A2}$$

where $\mathbf{u} = (u_1,u_2,u_3)^T$, $\hat{D} = DE$, E is the unit matrix, A is the constant matrix, and

$$A = \begin{pmatrix} 1 & 0 & 0\\ -1 & k_4 & 0\\ 0 & 0 & k_6 \end{pmatrix}$$

contains terms of the order of two and higher. Rewritten in the vector form, the boundary conditions are

$$\left.\frac{\partial \mathbf{u}}{\partial x}\right|_{\substack{x=0\\x=L}} = 0.$$

Let us introduce the following scalar product in the function space in $[0,L]$:

$$(\mathbf{f},\mathbf{g}) = \int_0^L \left(\sum_{i=1}^{3} f_i g_i\right) dx$$

and the norm $\|\mathbf{f}\| = (\mathbf{f},\mathbf{f})^{1/2}$.

Then, the stability of the system with respect to small perturbations can be studied by the perturbation method.[32–35]

If $\mathbf{u}_0$ is the stationary spatially nonuniform solution to system (A2) and $\mathbf{u} = \mathbf{u}_0 + \mathbf{z}$, $\|\mathbf{z}\| \ll \|\mathbf{u}_0\|$, $\mathbf{u}$ is the solution to the perturbed problem, the following equality can be derived:

$$\begin{aligned}
0 &= \left(\frac{\partial}{\partial t} - \hat{D}\frac{\partial^2}{\partial x^2} + A\right)\mathbf{u} + \mathbf{f}(\mathbf{u}) - \left(\frac{\partial}{\partial t} - \hat{D}\frac{\partial^2}{\partial x^2} + A\right)\mathbf{u}_0 - \mathbf{f}(\mathbf{u}_0)\\
&= \left(\frac{\partial}{\partial t} - \hat{D}\frac{\partial^2}{\partial x^2} + A\right)\mathbf{z} + \frac{\partial \mathbf{f}}{\partial \mathbf{u}}(\mathbf{u}_0)\cdot\mathbf{z} + O(\|\mathbf{z}\|^2).
\end{aligned}$$

Neglecting the second- and higher-order terms in $\mathbf{z}$, we can describe the evolution of the perturbation by the following set of equations:

$$\left(\frac{\partial}{\partial t} - \hat{D}\frac{\partial^2}{\partial x^2} + A\right)\mathbf{z} + \frac{\partial \mathbf{f}}{\partial \mathbf{u}}(\mathbf{u}_0)\cdot\mathbf{z} = 0, \tag{A3}$$

with the initial condition $\mathbf{z}_0$ (which is the perturbation experienced by the stationary spatially nonuniform solution $\mathbf{u}_0$ at $t=0$).

Let us consider the following functional:

$$\mathbf{J}=\frac{\|\mathbf{u}\|^2}{2}=\frac{1}{2}(\mathbf{u},\mathbf{u})$$

and its first variation

$$\delta\mathbf{J}=(\mathbf{u}_0,\mathbf{z}(\mathbf{t})). \tag{A4}$$

The stability of the stationary solution can be evaluated from the value of the first variation of this functional.

Using the Cauchy–Bunyakovskii inequality, we can write

$$|\delta\mathbf{J}|=\frac{2(\mathbf{u}_0,\mathbf{z}(t))}{\|\mathbf{u}_0\|^2}\leqslant 2\frac{\|\mathbf{z}(\mathbf{t})\|}{\|\mathbf{u}_0\|}\to 0$$

for $t\to\infty$ if the stationary spatially nonuniform solution is stable.

Let us consider the equation conjugate to (A3) (the associated equation)

$$\left(-\frac{\partial}{\partial t}-\hat{D}\frac{\partial^2}{\partial x^2}+A^*\right)\mathbf{w}+\left[\frac{\partial\mathbf{f}}{\partial\mathbf{u}}(\mathbf{u}_0)\right]^*\cdot\mathbf{w}=0, \tag{A5}$$

$\mathbf{w}|_{t=T}=\mathbf{w_T}=\mathbf{p}^*$. Here, T denotes the parameter, the value of $\mathbf{p}^*$ will be specified later, A^* is the matrix conjugate to A, and $[(\partial\mathbf{f}/\partial\mathbf{u})(\mathbf{u}_0)]^*$ is the matrix conjugate to the Jacobian matrix.

Let us scalarly multiply (A5) and (A3) by $\mathbf{z}$ and $\mathbf{w}$, respectively, and then subtract the latter product from the former. After integration of the remainder from 0 to T, we obtain

$$\int_0^T\left[\left(\mathbf{w},\frac{\partial\mathbf{z}}{\partial t}\right)+\left(\frac{\partial\mathbf{w}}{\partial t},\mathbf{z}\right)\right]dt-\int_0^T\left\{\left(\mathbf{w},\left[-\hat{D}\frac{\partial^2}{\partial x^2}+A+\frac{\partial\mathbf{f}}{\partial\mathbf{u}}\right]\mathbf{z}\right)-\left(\left[-\hat{D}\frac{\partial^2}{\partial x^2}+A^*+\frac{\partial\mathbf{f}^*}{\partial\mathbf{u}}\right]\mathbf{w},\mathbf{z}\right)\right\}dt=0.$$

The second term on the left-hand side of the equality is identically equal to zero, because (1) the operators are conjugate, and (2) the boundary conditions were chosen correspondingly. Therefore,

$$\int_0^T\left[\left(w,\frac{\partial\mathbf{z}}{\partial t}\right)+\left(\frac{\partial\mathbf{w}}{\partial t},\mathbf{z}\right)\right]dt=\int_0^T\left[\frac{\partial}{\partial t}(\mathbf{w},\mathbf{z})\right]dt$$
$$=(\mathbf{w},\mathbf{z})|_0^T$$
$$=(\mathbf{w_T},\mathbf{z}(T))-(\mathbf{w}_0,\mathbf{z}_0)=0.$$

The following identity is obtained:

$$(\mathbf{w}_0,\mathbf{z}_0)=(\mathbf{w_T},\mathbf{z}(T)). \tag{A6}$$

Let $\mathbf{w_T}=\mathbf{u}_0$ [$\mathbf{w}_0$ is the solution to conjugated problem (A5) at $t=0$; $\mathbf{z}_0$ is the perturbation to problem (A3) at $t=0$; and $\mathbf{z}(T)$ is the evolution of the perturbation by the moment $t=T$]. Then, if the structure is stable

$$(\mathbf{w}_0,\mathbf{z}_0)=\delta\mathbf{J}\to 0 \quad \text{as} \quad T\to\infty \quad \text{for} \quad \forall\mathbf{z}_0:\|\mathbf{z}_0\|\leqslant\delta.$$

Obviously, this is possible if $\|\mathbf{w}_0\|\to 0$ as T tends to infinity.

Now, using the earlier considerations, let us analyze the stationary spatially nonuniform solution to set (A1) for stability. To do this, we should solve the set conjugate to set (A1). The constitution $\tau=T-t$ converts the set conjugated to set (A1) to the following set of parabolic equations:

$$\frac{\partial w_1}{\partial\tau}-Dw_{1xx}''+w_1-w_2+g_{11}(x)w_1+g_{13}(x)w_3=0,$$

$$\frac{\partial w_2}{\partial\tau}-Dw_{2xx}''+K_4w_2+g_{21}(x)w_1=0,$$

$$\frac{\partial w_3}{\partial\tau}-Dw_{3xx}''+K_6w_3+g_{31}(x)w_1=0. \tag{A7}$$

For this set, the initial conditions ($\tau=0$ or $t=T$) are as follows: $w_1|_{\tau=0}=u_{10}$, $w_2|_{\tau=0}=u_{20}$, $w_3|_{\tau=0}=u_{30}$. This choice of initial conditions imposed on set (A7) specifies the unknown functions $\mathbf{p}^*$ as $\mathbf{w}|_{\tau=0}=\mathbf{p}^*=\mathbf{u}_0$.

Functions g_{ij} may be derived from (A5):

$$g_{11}(x)=\left.\frac{\partial f_1}{\partial u_1}\right|_{\mathbf{u}=\mathbf{u}_0}$$
$$=-\frac{K_1u_{20}}{1+K_3u_{30}}[1-2u_{10}+2K_2u_{10}-3K_2u_{10}^2],$$

$$g_{12}(x)=\left.\frac{\partial f_2}{\partial u_1}\right|_{\mathbf{u}=\mathbf{u}_0}=0,$$

$$g_{13}(x)=\left.\frac{\partial f_3}{\partial u_1}\right|_{\mathbf{u}=\mathbf{u}_0}=-2K_5u_{10},$$

$$g_{21}(x)=\left.\frac{\partial f_1}{\partial u_2}\right|_{\mathbf{u}=\mathbf{u}_0}=-K_1(1-u_{10})\frac{1+K_2u_{10}}{1+K_3u_{30}}u_{10},$$

$$g_{31}(x)=\left.\frac{\partial f_1}{\partial u_3}\right|_{\mathbf{u}=\mathbf{u}_0}=K_1K_3u_{10}u_{20}\frac{(1-u_{10})(1+K_2u_{10})}{(1+K_3u_{30})^2}.$$

Let us study the discrete analogue of the norm $\|\mathbf{w}(t)\|$:

$$\sum_{i=0}^{N}(w_{1i}^2+w_{2i}^2+w_{3i}^2)h=\|\mathbf{w}(t)\|_h^2,$$

where h is the space discretization step of a difference grid, $N=(L/h)$.

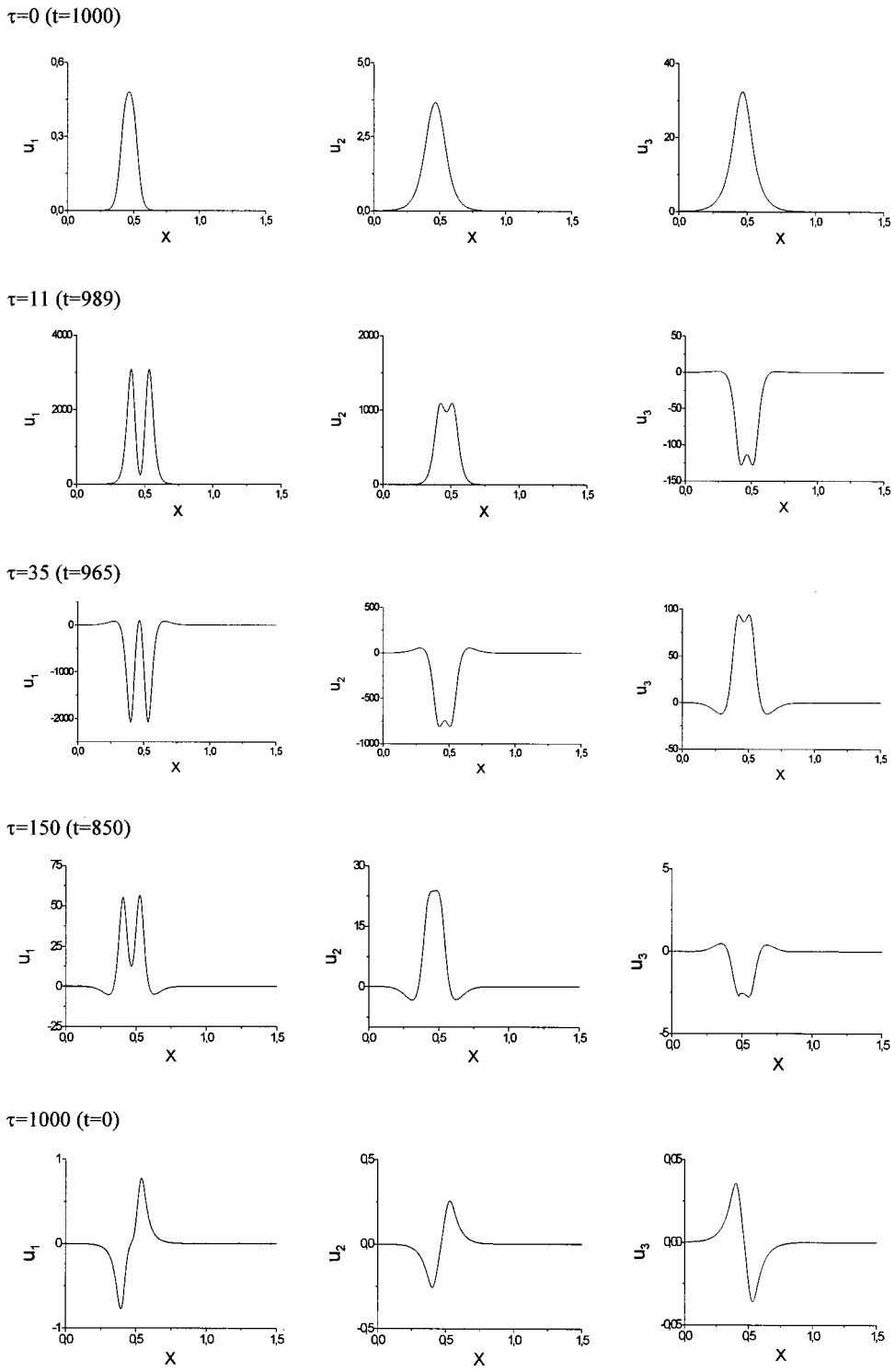

FIG. 13. Temporal evolution of the solution to the conjugate system linearized in the vicinity of its steady-state solution.

The conjugate set was used to characterize the response of the original system to small perturbations.[32] A typical evolution of the solution of the conjugate set is shown in Fig. 13. The solution to the conjugate problem is localized to a finite support for each moment of time, i.e., is nonzero only in the interval located far from the boundaries of the area under consideration. This interval is much shorter than the spatial size of the problem.

Figure 14 shows how the norm depends on time. The value of the norm $\|\mathbf{w}(\tau)\|_h$ increases steeply with time (by approximately 90 times) and then diminishes to almost zero. Evidently, upon $T\to\infty$ $\|\mathbf{w}(t)\|_h|_{t=0,\tau=T}=\|\mathbf{w}_0\|_h\to 0$, i.e., such solutions are stable (in the linear approximation).

It is also clear that the stationary pulse should be stable upon collision with the moving pulse, because the value of functional (A4) is equal to zero at any moment of time. If the perturbation is located in the region where the solution of the conjugate equation differs from zero and the value of integral (A4) or (A6) for the initial perturbation is large, the small-perturbation approach can become invalid, and the pulse amplitude can reach the subthreshold values.

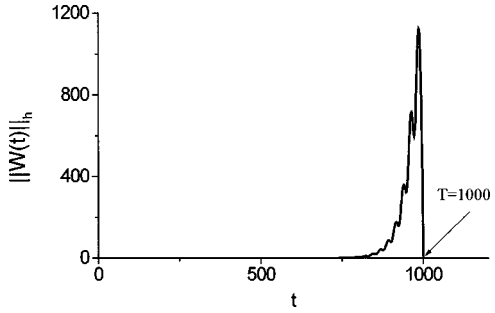

FIG. 14. Temporal evolution of the norm of the solution to conjugate set (A7).

APPENDIX B: THE EXISTENCES OF SPATIALLY NONUNIFORM STATIONARY SOLUTIONS

First, let us consider the following auxiliary boundary-value problem for system (2.25):

$$\begin{aligned} u''_{1xx} &= u_1 - K_1 u_1 u_2 (1-u_1)\frac{(1+K_2 u_1)}{(1+K_3 u_3)}, \\ u''_{2xx} &= -u_1 + K_4 u_2, \\ u''_{3xx} &= -K_5 u_1^2 + K_6 u_3 \end{aligned} \tag{B1}$$

with the boundary conditions $\mathbf{u}(0)=\mathbf{A}$, $\mathbf{A}=(A_1,A_2,A_3)^T$, $\mathbf{u}(L)=\mathbf{0}$, and additional constraints taken in the form $(\partial\mathbf{u}/\partial x)(0)=\mathbf{0}$, $(\partial\mathbf{u}/\partial x)(L)=\mathbf{0}$.

Here, L is the semisize of the structure; the value of L will be specified later. Suppose that all functions, which are examined in this section, belong to space $C^2\ [0,L]$.

Let us introduce a number of ancillary functions (B2):

$$\begin{aligned} &\rho_{11}=u_1(x)-\beta_1(x), \quad \beta_1(x)=A_1\exp\left(-\frac{5\pi^2}{16l^2}x^2\right), \\ &\rho_{12}=u_2(x)-\beta_2(x), \quad \beta_2(x)=A_2\exp\left(-\frac{\pi^2}{4L^2}x^2\right), \\ &\rho_{13}=u_3(x)-\beta_3(x), \quad \beta_3(x)=A_3\exp\left(-\frac{\pi^2}{4L^2}x^2\right), \\ &\rho_{21}=\alpha_1(x)-u_1(x), \\ &\alpha_1(x)=\begin{cases} 0, & l<x\leqslant L \\ A_1\left[\cos^2\dfrac{\pi x}{2l}-\dfrac{\pi^2}{16l^6}x^2(x+l)^2(x-l)^2\right], & x\leqslant l, \end{cases} \\ &\rho_{22}=\alpha_2(x)-u_2(x), \quad \alpha_2(x)=A_2\cos^2\frac{\pi x}{2L}, \\ &\rho_{23}=\alpha_3(x)-u_3(x), \quad \alpha_3(x)=A_3\cos^2\frac{\pi x}{2L}. \end{aligned} \tag{B2}$$

Here, A_1, A_2, A_3, and $l\ (0<l<L)$ denote the positive parameters whose estimates will be obtained below. It easy to test directly that $\alpha_1(x)\in C^2[0,L]$. All functions α_i and β_i are not negative. For $x=0$, all functions α_i and β_i exhibit maxima equal to A_i, $i=1,2,3$. In addition, $\beta_i(x)\geqslant\alpha_i(x)$ $\forall x\in[0,L]$. The right-hand sides of the system (B1) do not depend explicitly on the first derivatives $\mathbf{u}'_x$ and, consequently, satisfy the Nagumo conditions.[36,37] By the theorem proved in Ref. 37, auxiliary problem (B1) has a solution $\mathbf{u}=[u_1(x),u_2(x),u_3(x)]^T$. If

$$\alpha''_k x \geqslant F_k(x,\mathbf{u}) \tag{B3}$$

at all points x where $\mathbf{u}(x)=\alpha(x)$ and $\mathbf{u}'(\mathbf{x})=\alpha'(x)$, and if

$$\beta''_k x \leqslant F_k(x,\mathbf{u}) \tag{B4}$$

at all points x where $\mathbf{u}(x)=\beta(x)$ and $\mathbf{u}'(\mathbf{x})=\beta'(x)$, the solution is bounded by function (B2):

$$\begin{aligned} &\alpha_1(x)\leqslant u_1(x)\leqslant\beta_1(x), \\ &\alpha_2(x)\leqslant u_2(x)\leqslant\beta_2(x), \\ &\alpha_3(x)\leqslant u_3(x)\leqslant\beta_3(x). \end{aligned}$$

These conditions are satisfied at the right boundary of L for all non-negative functions $\mathbf{u}(x)$. At $x=0$, conditions (B3) and (B4) lead to the set of coefficient equalities, which can be considered as a set of three equations in five unknowns:

$$\begin{aligned} &\left(\frac{5\pi^2}{8l^2}+1\right)=K_1A_2(1-A_1)\frac{(1+K_2A_1)}{(1+K_3A_3)}, \\ &\left(\frac{\pi^2}{2L^2}+K_4\right)A_2=A_1, \\ &\left(\frac{\pi^2}{2L^2}+K_6\right)A_3=K_5A_1^2. \end{aligned} \tag{B5}$$

Let A_1 and L be parameters of set (B5). This gives

$$A_2=\frac{A_1}{(\xi+K_4)}, \quad A_3=\frac{K_5A_1^2}{(\xi+K_6)},$$

where $\xi=(\pi^2/2L^2)$. Substituting these values into the first equation of set (B5), we obtain the equality relating to l, $A_1$and ξ:

$$\begin{aligned} \left(\frac{5\pi^2}{8l^2}+1\right)=K_1\frac{A_1}{(\xi+K_4)}(1-A_1) \\ \times\frac{(1+K_2A_1)}{[1+K_3K_5A_1^2/(\xi+K_6)]}. \end{aligned} \tag{B6}$$

If the maximum of the right-hand side of (B6) in A_1 exceeds $(5\pi^2/8l^2)+1$ at a fixed halfwidth of the structure L, then the spatially nonuniform stationary solution exists.

Omitting further calculations, we summarize that if conditions (B7) are satisfied, the size of L is bounded from both above and below:

$$\left(\frac{5\pi^2}{8l^2}+1\right)<\frac{K_1A_1(1-A_1)(1+K_2A_1)}{K_4+K_6+K_3K_5A_1^2},$$
$$\left(\frac{5\pi^2}{8l^2}+1\right)>\frac{K_6K_1A_1(1-A_1)(1+K_2A_1)}{K_4(K_6+K_3K_5A_1^2)}. \tag{B7}$$

Thus, if conditions (B5) are satisfied, the spatially nonuniform stationary solutions exist.

Since set (B1) is invariant with respect to the substitution $x\rightarrow -x$, the solution can be evenly extended into $[-L,L]$. This solution belongs to $C^2[-L,L]$ because of the additional condition $(\partial\mathbf{u}/\partial x)(0)=\mathbf{0}$ and can be merged with the solution $\mathbf{u}\equiv\mathbf{0}$ because $(\partial\mathbf{u}/\partial x)(L)=\mathbf{0}$, and the condition of flux continuity is, therefore, satisfied.

Now, the construction algorithm for the nonuniform stationary solution to the original problem is evident. After substituting $\eta=x-r$, where r is the point of the structure maximum (a coordinate), and $\varphi=(\eta/\sqrt{D})$, we obtain auxiliary problem (B5) in the vicinity of $\varphi=0$. For $|\varphi|>L$ the solution is assumed to be zero.

Numerical experiments give the regime, in which equality (B5) is satisfied to the accuracy of several percents, and the structure width L is of the maximum possible value.

Note that the qualitative behavior of the point system $(D\equiv 0)$ does not depend on whether the original set was reduced to a system of two $[(\partial u_2/\partial t)\equiv 0]$ or three equations. However, analysis shows that, in the case of two equations in the final system, the stationary spatially nonuniform solutions of this type do not exist.

[1] A. M. Turing, ''The chemical basis of morphogenesis,'' Philos. Trans. R. Soc. London, Ser. B **237**, 37–42 (1952).

[2] G. Nicolis and I. Prigogine, *Self-Organization in Non-Equilibrium Systems* (Wiley, New York, 1977).

[3] *Oscillation and Traveling Waves in Chemical Systems*, edited by R. J. Field and M. Burger (Wiley, New York, 1985).

[4] H. Meinhardt, ''Dynamics of stripe formation,'' Nature (London) **376**, 722–723 (1995).

[5] A. J. Koch and H. Meinhardt, ''Biological pattern formation: From basic mechanisms to complex structures,'' Rev. Mod. Phys. **66**, 1481–1507 (1994).

[6] K. J. Lee, W. D. McCormick, Q. Quyang, and H. L. Swinney, ''Pattern formation by interacting chemical fronts,'' Science **261**, 192–194 (1993).

[7] A. De Wit, ''Spatial patterns and spatiotemporal dynamics in chemical systems,'' Adv. Chem. Eng. **109**, 435–513 (1999).

[8] I. S. Lendyel and I. R. Epstein, ''Transient Turing structures in a gradient-free closed system,'' Science **259**, 493–495 (1993).

[9] J. Ross, A. Arkin, and S. C. Mueller, ''Experimental evidence of Turing structures,'' J. Phys. Chem. **99**, 10417–10419 (1995).

[10] F. I. Ataullakhanov and G. T. Guriya, ''Spatial aspects of the dynamics of blood clotting—I. Hypothesis,'' Biophysics (Engl. Transl.) **39**, 91–97 (1994).

[11] F. I. Ataullakhanov, G. T. Guriya, V. I. Sarbash, and R. I. Volkova, ''Spatio-temporal dynamics of clotting and pattern formation in human blood,'' Biochim. Biophys. Acta. **1425**, 453–468 (1998).

[12] F. I. Ataullakhanov, G. T. Guriya, and A. Yu. Safroshkina, ''Spatial aspects of the dynamics of blood clotting—II. Phenomenological model,'' Biophysics (Engl. Transl.) **39**, 99–108 (1994).

[13] A. I. Lobanov, T. K. Starozhilova, and G. T. Guria, ''Numerical investigation of pattern formation processes in blood coagulation,'' Matematicheskoe modelirovanie **9**, 83–95 (1997); in Russian.

[14] V. I. Zarnitsina, A. V. Pokhilko, and F. I. Ataullakhanov, ''A mathematical model for the spatio-temporal dynamics of intrinsic pathway of blood coagulation. I. The model description,'' Thrombosis Research **84**, 225–236 (1996).

[15] V. I. Zarnitsina, A. V. Pokhilko, and F. I. Ataullakhanov, ''A mathematical model for the spatio-temporal dynamics of intrinsic pathway of blood coagulation. II. Results,'' Thrombosis Research **84**, 333–344 (1996).

[16] B. S. Kerner and V. V. Osipov, *Autosolitons* (Moscow, Nauka, 1991), in Russian.

[17] A. N. Zaikin, ''Generation, propagation, and interaction of excitons (autowave-particles) in an active medium,'' Preprint, Pushino (1993), in Russian.

[18] W. N. Reynolds, J. E. Pearson, and S. Ponce-Dawson, ''Dynamics of self-replicating patterns in reaction-diffusion systems,'' Phys. Rev. Lett. **72**, 2797–2800 (1994).

[19] K. J. Lee, W. D. McCormick, J. E. Pearson, and H. L. Swinney, ''Experimental observation of self-replicating spots in a reaction-diffusion system,'' Nature (London) **369**, 215–218 (1994).

[20] K. Krischer and A. Mikhailov, ''Bifurcation to travelling spots in reaction-diffusion system,'' Phys. Rev. Lett. **73**, 3165–3168 (1994).

[21] C. P. Schenk, M. Or-Guil, M. Bode, and H.-G. Purwins, ''Interacting pulses in three-component reaction-diffusion systems on two-dimensional domains,'' Phys. Rev. Lett. **78**, 3781–3784 (1997).

[22] D. T. Berg, M. R. Wileyand, and B. W. Grinnell, ''Enhanced protein C activation and inhibition of fibrinogen cleavage by a thrombin modulator,'' Science **273**, 1389–1391 (1996).

[23] Q. D. Dang, A. Vindigni, and E. Di Cera, ''Identification of residues linked to the slow-fast transition of thrombin,'' Proc. Natl. Acad. Sci. U.S.A. **91**, 11185–11189 (1995).

[24] J. W. Fenton, Jr., ''Regulation of thrombin generation and functions,'' Semin. Thromb. Hemost. **14**, 234–240 (1988).

[25] E. Hairer, S. P. Norsett, and G. Wanner, *Solving Ordinary Differential Equations. Nonstiff Problems*, Springer Series in Computational Mathematics 8 (Springer, Berlin, 1987).

[26] A. I. Tolstykh, *Compact Difference Schemes and Their Applications to Fluid Dynamics Problems* (Moscow, Nauka, 1990), in Russian.

[27] A. I. Khibnik, Yu. A. Kuznetsov, V. V. Levitin, and E. V. Nikolaev, 1993, LocBif, Version2: Interactive LOCal BIFurcation Analyzer, CAN Expertise Centre, Amsterdam, 1–148.

[28] B. N. Belintzev, B. F. Dibrov, M. A. Lifshitz, and M. V. Volkenshtein, ''Nonlinear stability in distributed trigger type system. Biological threshold,'' Biofizika **23**, 864–869 (1978), in Russian.

[29] Y. Oono and M. Kohmoto, ''Discrete model of chemical turbulence,'' Phys. Rev. Lett. **55**, 2927–2931 (1985).

[30] D. Feinn and P. Ortoleva, ''Catastrophe and propagation in chemical reactions,'' J. Chem. Phys. **67**, 2119 (1977).

[31] P. Ortoleva, ''J. Ross theory of propagation of discontinuities in kinetic systems with multiple time scales: Fronts, front multiplicity and pulses,'' J. Chem. Phys. **63**, 3398 (1975).

[32] G. I. Marchuk, ''Perturbation theory and the statement of inverse problems,'' Lect. Notes Comput. Sci. **4**, 159–166 (1973).

[33] G. I. Marchuk, V. I. Agoshkov, and V. P. Shutyaev, *Conjugated Equations and Perturbation Methods in Nonlinear Problems of Mathematical Physics* (Moscow, Fizmatlit, 1993), in Russian.

[34] G. I. Marchuk and V. I. Agoshkov, ''Conjugated operators and algorithms of perturbation in nonlinear problems. 1. Principles of construction of conjugated operators,'' Sov. J. Numerical Analysis Mathematical Modeling **1**, 21–46 (1988).

[35] G. I. Marchuk and V. I. Agoshkov, ''Conjugated operators and algorithms of perturbation in nonlinear problems. 2. Perturbation algorithms,'' Sov. J. Numerical Analysis Mathematical Modeling **2**, 115–136 (1988).

[36] M. Nagumo, ''Uber die differentialgleichung $y''=f(x,y,y')$,'' Proc. Phys. Math. Soc. Jpn. **19**, 861–866 (1937).

[37] K. W. Chang and F. A. Howes, *Nonlinear Singular Perturbation Phenomena: Theory and Applications* (Springer, New York, 1984), Vol. 56.